Bima Journal of Science and Technology, Vol. 8(3B) Oct, 2024 ISSN: 2536-6041

DOI: 10.56892/bima.v8i3B.844

Charge Carrier Dynamics and Bandgap Modulation in Doped $ZnWO_4$ Nanocomposites

Abubakar H. L.[1]*, Abubakar A. A.[2], Nasir Z. J.[3]

[1]Department of Chemistry, Nile University of Nigeria, Abuja, FCT, Nigeria.
[2]Department of Electrical and Electronics Engineering, Nile University of Nigeria, Abuja, FCT, Nigeria.
[3]Department of Microbiology, Nile University of Nigeria, Abuja, FCT, Nigeria.
Corresponding Authors: abubakarhassana25@gmail.com

ABSTRACT

This study investigates the effects of doping on the bandgap energy of synthesized and doped $ZnWO_4$ nanomaterials. The synthesized nanomaterials were doped with varying concentrations (1%, 3%, 5% & 7%) of the nonmetals nitrogen, carbon and boron. The optical, morphological and textural nature of the prepared nanomaterials were characterized by different analytical tools. The UV-Visible/HRTEM/XRD analysis confirmed that the incorporation of the dopants which had an impact on the band gap energy but did not significantly alter the host material's phase or produce defects, the orientation and growth pattern of the doped $ZnWO_4$ along [021] plane was observed. There was an observed decrease in the bandgap energy upon doping from 4.68 eV to 2.31 eV, 2.0 eV and 2.30 eV for 7%N-$ZnWO_4$, 7%C-$ZnWO_4$ and 7%B-$ZnWO_4$. There was also an increase in the relative crystallinity of the nanocomposite materials. The XRD results obtained showed a decrease in crystallite size of most of the nanomaterials with the lowest for each dopant being 8.11 nm, 7.64 nm, 7.25 nm for 1%N, 3%C and 3%B respectively, the XRD results also corroborated with the HRTEM results obtained. The results from the characterization revealed that doping was successful at improving the efficiency of the synthesized $ZnWO_4$ nanoparticles.

Keywords: $ZnWO_4$ nanoparticles, doping, bandgap

INTRODUCTION

Nanotechnology is the manipulation of matter at the scale of 1–100 nm to create functional materials, devices, and systems. Operating at the molecular level, it enables the precise assembly of structures atom by atom, resulting in novel molecular arrangements with unique properties. The field encompasses the design, fabrication, and application of nanostructures and nanomaterials, with the primary goal of understanding the relationship between material dimensions and their physical, chemical, and mechanical properties. A nanometer (nm), equivalent to one billionth of a meter (10−9 m), represents the core measurement of this science (Ali, 2020). Materials in bulk form vary in their structural classifications—metals, semiconductors, and insulators—each influencing their electrical, optical, and mechanical properties in different ways. These properties are essential to determining the behavior and applications of materials across various fields (Ali, 2020; Srinivasan *et al.,* 2016). The rapid growth of nanotechnology has driven the development of nanomaterials such as nanoparticles, nanofibers, nanofilms, and nanoblocks, which are now widely integrated into numerous industries and everyday applications. When conventional materials are processed at the nanoscale, quantum effects lead to significant alterations in their surface, volume, optical, thermal, electrical, magnetic, and mechanical characteristics (Su *et al.,* 2021).

To enhance the performance of pure $ZnWO_4$ nanoparticles, various strategies have been explored, including surface modification, composite formation, tuning of energy band

DOI: 10.56892/bima.v8i3B.844

gaps, and the incorporation of rare-earth (RE) elements, metals, and non-metals. These approaches have proven highly effective in improving the photocatalytic efficiency of $ZnWO_4$ nanoparticles (Geetha *et al.,* 2022). In recent years, the synthesis of a broader range of nanomaterials has increased significantly, both in diversity and production scale. This growth necessitates the development of more precise and reliable protocols for characterizing these materials. However, the characterization of nanoscale materials remains challenging due to their small size and the limited quantities typically produced in laboratory settings, which complicates comprehensive analysis compared to bulk materials (Mourdikoudis *et al*., 2018). In this study, $ZnWO_4$ nanoparticles were synthesized and enhanced through doping with nitrogen, carbon, and boron to improve their properties. The modifications were analyzed to determine the optimal concentration of dopants for maximizing the performance of $ZnWO_4$ nanoparticles.

MATERIALS AND METHODS

Synthesis of $ZnWO_4$ nanoparticles

The method presented by Abubakar *et al*. (2023) was adopted with slight modifications. In simple terms, 250 cm^3 of an equal mixture of ethanol and distilled water was used to dissolve 25 g of zinc acetate dehydrate. Once the salt had completely dissolved, the mixture was swirled. Similarly, a 250 cm^3 beaker was filled with an equal amount of distilled water and ethanol to dissolve 15 g of sodium tungsten. After that, the mixture was swirled to ensure that the salt was completely dissolved. Additionally, 50 cm^3 of each of the sodium tungstate and zinc acetate solutions from two different beakers were transferred into a 500 cm^3 beaker. Using a solution of 2 M HCl and 2 M NaOH, the pH was stabilised. Using a magnetic stirrer set at 2000 rpm, a packing ice cube was placed near the beaker to aid in temperature lowering. After leaving the resulting gel for half an hour, it was cleaned with a 75:25 mixture of ethanol and water to get rid of any remaining ions, and it was then dried for twenty-four hours at 100 °C. After being taken out of the oven, the sample was pulverised with a pestle and mortar in a laboratory setting before being calcined at 400 °C. The calcined sample that was obtained was kept in an airtight bottle with the label $ZnWO_4$.

Doping of $ZnWO_4$ nanocomposite

In the end, 1%C-$ZnWO_4$ nanoparticles were synthesized using the wet impregnation method. In this instance, a 250 cm^3 beaker was filled with 3 g of the synthesised $ZnWO_4$ nanoparticles, 50 cm^3 of 1% PEG solution was added gradually, and the mixture was stirred for 3 h at 500 rpm using a magnetic stirrer. The mixture was then aged for 6 h, rinsed many times with a water/ethanol mixture, oven dried for an entire night at 80°C, and then calcined for 2 h in a furnace at 400°C. The same process was used to synthesize 3%, 5%, and 7% C-$ZnWO_4$ nanoparticles by synthesising corresponding PEG solutions. The synthesis of 1%, 3%, 5%, and 7% N-$ZnWO_4$ and B-$ZnWO_4$ was also carried out using this method. As sources of N and B integrated onto the lattice layer of $ZnWO_4$ nanoparticles, NH_3 and H_3BO_3 were used separately, in contrast to C-$ZnWO_4$, where PEG was used as the C-precursor. Using the High Resolution Transmission Electron Microscope (HRTEM), Selected Area Electron Diffraction (SAED), and X-ray Diffraction (XRD) spectroscopy, the synthesised materials were characterised. The material with the least band gap energy and small crystallite size was used to determine the optimum dopant concentration (Rahmani and Sedaghat, 2019; Geetha *et al*., 2022).

RESULTS AND DISCUSSION

DOI: 10.56892/bima.v8i3B.844

Characterization of Doped $ZnWO_4$ Nanoparticles

In order to identify the ideal dopant concentration on the lattice of the host material, $ZnWO_4$ nanoparticles were doped with 1%, 3%, 5%, and 7% of certain non-metals (N, C, and B). The resulting $ZnWO_4$ nanocomposites were then studied using HRTEM, SAED, UV-visible spectroscopy, and XRD.

UV-Visible Analysis and Bandgap Measurements of doped $ZnWO_4$ Nanoparticles

The Figure 1 (aii-cii) shows the results of UV-visible measurements taken at wavelengths between 200 and 650 nm to assess the effect of doping with N, C, and B at concentrations of 1%, 3%, 5%, and 7%. While equation 1 (ai-ci) displays the corresponding Tauc's plots, the band gap energies were estimated. Tauc's equation 2 was used to determine the doped $ZnWO_4$ nanocomposites' optical bandgap energy. According to Geetha *et al.* (2021), there is a correlation between the semiconductors' incident photon energy and the absorption coefficient.

$$khv=B(hv–Eg)^2 \qquad (1)$$

In this instance, the exponent n is interpreted as an indirect bandgap, Eg refers the optical bandgap of the material, and 2 is the index. B is the constant known as the band tailing parameter. For each sample, the band gap energy (Eg) is calculated by plotting 1/2 against hv and extrapolating the linear component. The absorption spectra edge may have undergone a red shift, or moved slightly to a higher wavelength when individual non-metals (B, C, and N) were doped onto $ZnWO_4$ lattice layers, as seen in Figure 3.1 (aii, bii, and cii). Adesoye *et al.* (2022) presented a rise in the dopant ion concentration being associated with an increase in the red shift. This shift was caused by a number of variables, including changes in the particle size of the material, lattice strain, and oxygen deprivation. According to these light absorption spectra, visibility increased as the amounts of dopants increased (Aga *et al.,* 2022).

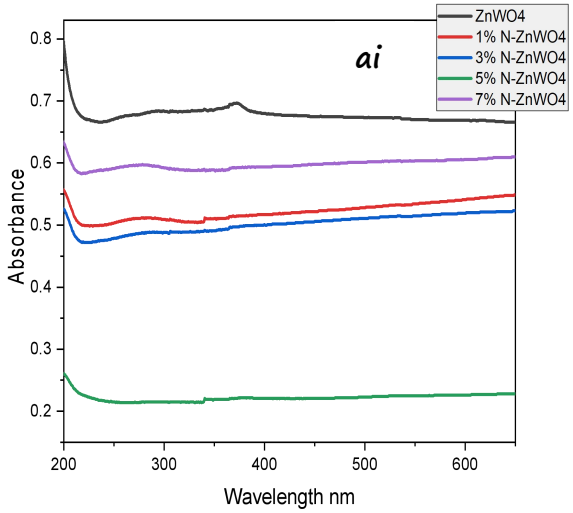

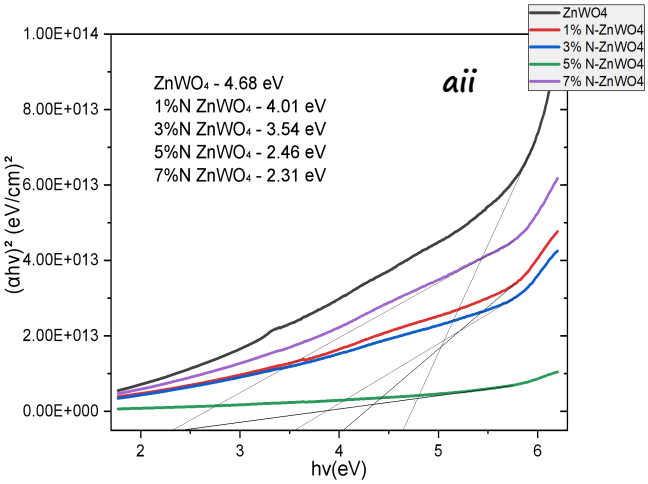

Bima Journal of Science and Technology, Vol. 8(3B) Oct, 2024 ISSN: 2536-6041

DOI: 10.56892/bima.v8i3B.844

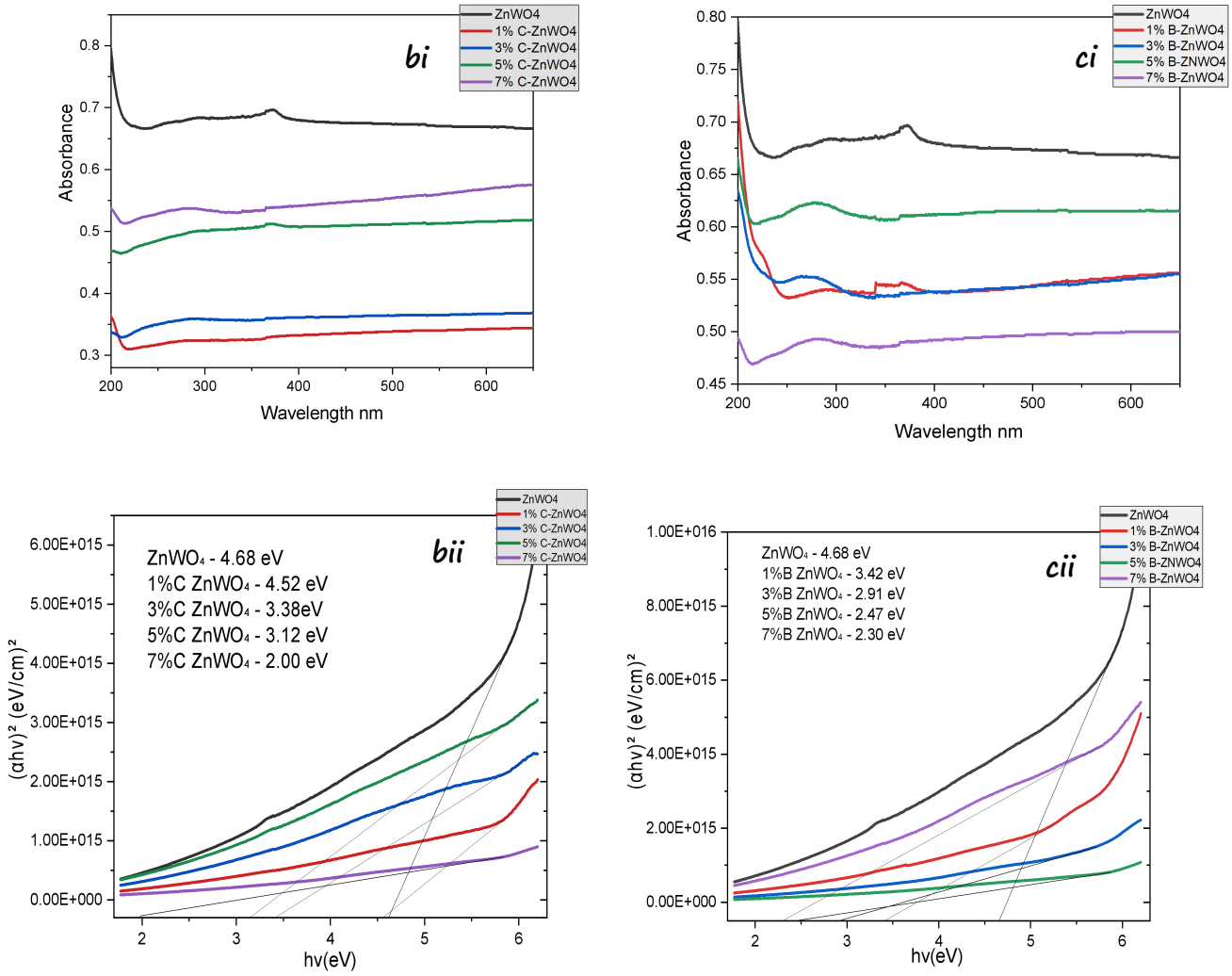

Figure 1 (a-c): Tauc's plot and UV-Visible spectras of the $ZnWO_4$ nanocomposites

Plate I displays SAED patterns and High Resolution Transmission Electron Microscopy (HRTEM) micrographs of the synthesised N, C, and B doped $ZnWO_4$ nanoparticles at high (2 nm) and low (50 nm) magnification.

HRTEM and SAED of N, C and B doped $ZnWO_4$ nanocomposites

DOI: 10.56892/bima.v8i3B.844

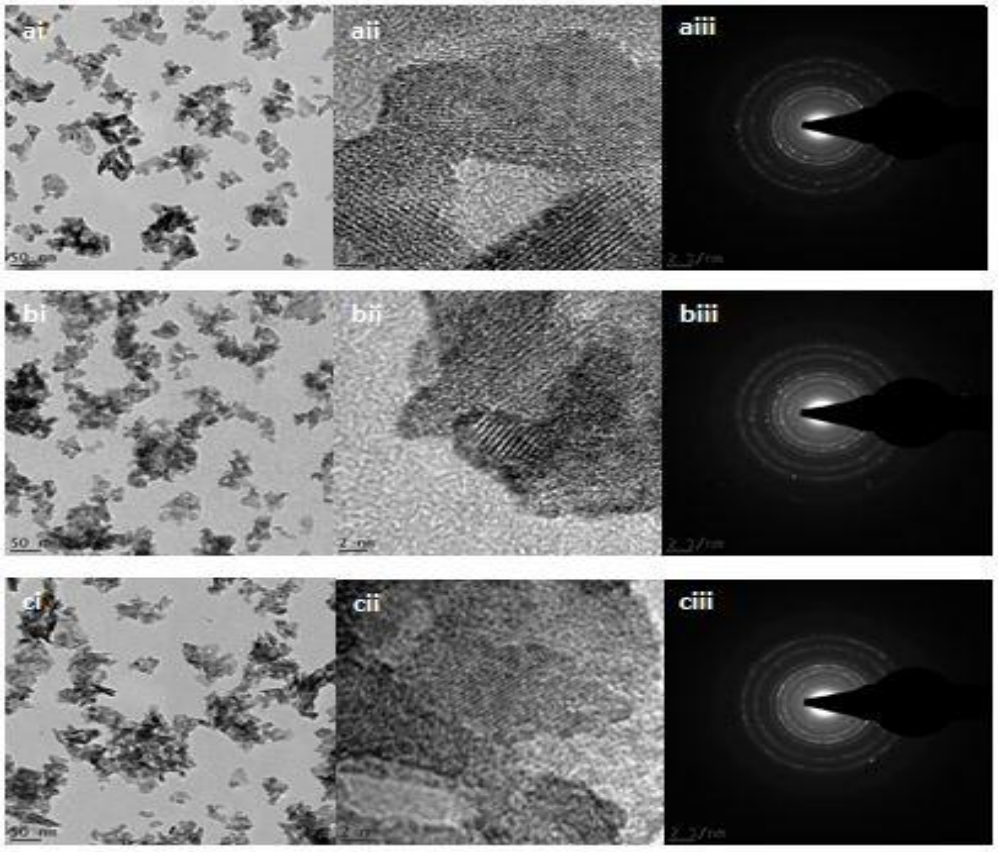

Plate I (a-c): HRTEM and SAED images doped $ZnWO_4$ composites

X-Ray Diffraction Patterns for Doped $ZnWO_4$ Nanocomposites

The phase structure of the doped $ZnWO_4$ nanocomposites was studied using XRD technique and the spectrum obtained is presented in Figure 2 (a-c). According to Dutta and Raval (2018), all doped nanocomposites obtained have a space group of p2/c and a monoclinic phase of zinc tungsten oxide (ZnWO4) with JCPDS no. 15-0554. This is because the synthesis and calcination temperatures of both the doped nanocompoites and pure $ZnWO_4$ nanoparticles remained constant. X-ray diffraction (XRD) was used to investigate the mineralogical phase and the crystalline nature of $ZnWO_4$ nanocomposites doped with non-metals (N, C, and B). The corresponding patterns are shown in Figure 2 (a-c).

Debye Scherrer's Equation was used to determine the exact locations of the main peaks and to calculate the crystallite sizes of each nanocomposite:

$$d = \frac{k\lambda}{\beta\cos\theta} \qquad \text{Equation 1}$$

DOI: 10.56892/bima.v8i3B.844

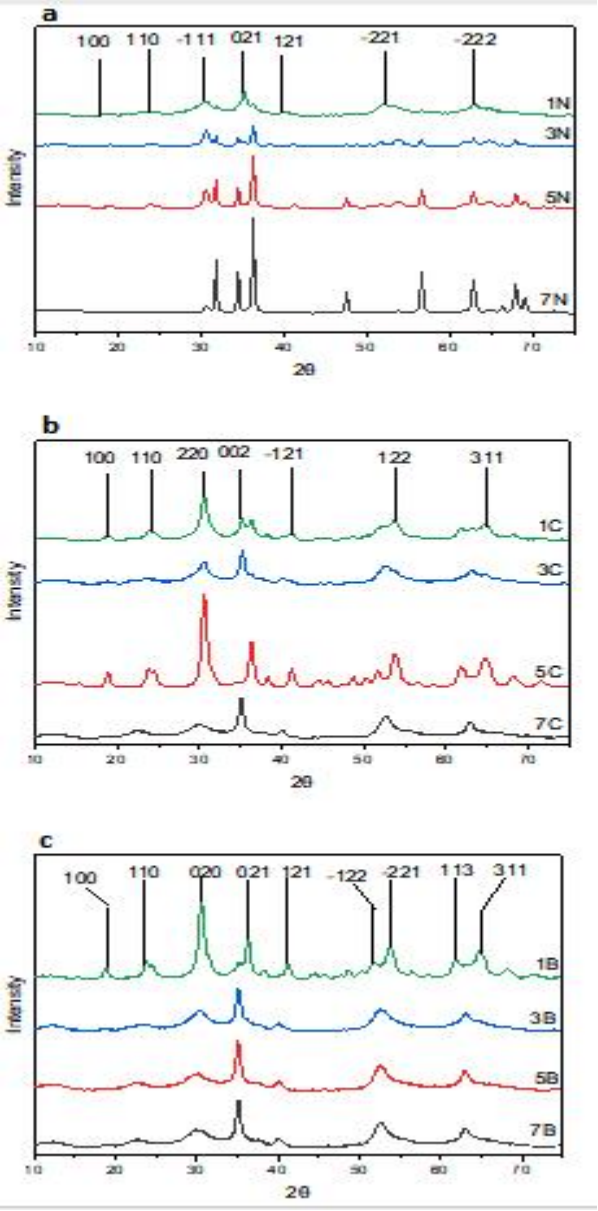

Figure 2 (a-c): X-ray diffraction patterns doped $ZnWO_4$ nanocomposites

DISCUSSION

The synthesised $ZnWO_4$ nanoparticles have an estimated bandgap energy of 4.68 Ev, which is within the stated range for $ZnWO_4$ (Kumar *et al*., 2022). Bandgap energy was found to have drastically decreased upon doping, with the lowest values for each dopant being 2.31 Ev for 7%N-$ZnWO_4$, 2.00 Ev for 7%C-$ZnWO_4$, and 2.30 Ev for 7%B-$ZnWO_4$. This demonstrated unequivocally that doping not only lowered the bandgap energy of $ZnWO_4$, but also that incorporation of these metal and nonmetal ions into the lattice of $ZnWO_4$ causes the band gap energy to fall with increasing dopant concentration. Because doping lowers conducting level of $ZnWO_4$ by introducing acceptor energy levels, doped $ZnWO_4$—both metal and non-metal—is predicted to have significantly greater solar energy conversion efficiencies than undoped $ZnWO_4$. Additionally, this will promote charge carrier separation and decrease photogenerated electron-hole pair recombination, extending the carriers' lifespan (Chakraborty *et al*., 2021). In this instance, less energy is needed to excite the valence electrons, which would therefore speed up the synthesised nanocomposites' photocatalytic activity (Geetha *et al.* 2021).

The shape and crystalline nature of the material, as well as the type of dopant ions present in the matrix, may be responsible for the variations in bandgap energy between the doped and undoped nanomaterials. In comparison to the undoped equivalent, the doped samples' generation of new crystal defects and localised states may also be connected to the decrease in bandgap energy (Tijani *et al.,* 2021). The development of uniformly dispersed agglomerated spherical particles is demonstrated by the HTREM micrographs for B, C, and N doped $ZnWO_4$.The areas of the dopant that are successfully doped are shown by the darker spots in $ZnWO_4$ nanocomposites (Rahmani and Sedaghat, 2019). Regardless of the dopant, a similar morphology was seen. This could be because electrons from the identical 2p orbitals of B, C, and N were transported to the $ZnWO_4$ host lattice (Rahmani and Sedaghat, 2019). Bright spots and lattice fringes were visible in the selected area electron diffraction (SAED) micrographs of the doped $ZnWO_4$

DOI: 10.56892/bima.v8i3B.844

nanocomposites and low magnification HRTEM micrographs. This demonstrates unequivocally that N, C, and B doped $ZnWO_4$ nanocomposites have a reasonably high crystalline nature.

For each nanocomposite material, the crystallinity correlates with the XRD patterns (Raizada et al, 2017), regardless of the dopant, the SAED micrographs of the nanomaterials showed that they are extremely polycrystalline in nature (Raizada *et al*., 2017). The addition of N, C, and B undoubtedly resulted in additional flaws and certain distortions of the $ZnWO_4$ lattice fringes (Abubakar *et al.,* 2022; Sethi *et al*., 2018). The main characteristic peaks of the N-doped $ZnWO_4$ nanocomposite were found at 18.90°, 24.57°, 30.72°, 36.31°, 41.14°, 53.99°, and 63.38° of 2θ, which corresponds to the crystal planes (100), (110), (111), (021), (121), (221), and (222). This can be indexed as JCP2: 00-036-1451, the hexagonal zincite phase. It is clear that the pattern and orientation of the peaks changed dramatically as the concentration of N grew. This was caused by the dopant dislodging Zn, which led to the creation of the N_4W_5 phase rather than $ZnWO_4$. A new plane (030) emerged at 47.67° and grew larger as the concentration increased, while numerous diffraction peaks disappeared due to Zn being replaced by N. The peak at 2 θ value of 36.31° considerably expanded with rising N concentration. The average crystallite diameters for the $ZnWO_4$ nanocomposite doped with 1%, 3%, 5%, and 7% N were determined to be 8.11 nm, 10.80 nm, 20.29 nm, and 20.17 nm. Similar findings were noted and reported by Sagheer *et al.* (2020), and in this instance, the crystallite size grew as the concentration of N increased, this is because the dopant ions were incorporated onto the $ZnWO_4$ lattice.

The predominant peaks for the C-doped $ZnWO_4$ nanocomposite emerged at 2θ at 18.90°, 24.57°, 36.32°, 36.43°, 41.32°, 52.53°, and 64.35°.These correspond to the crystal planes (100), (110), (020), (002), (-121), (122), and (311), and the substance that was created is a part of the monoclinic phase of Z nWO_4. The phase of $ZnWO_4$ was unaffected by the presence of C. The mean crystallite dimensions for the $ZnWO_4$ nanocomposite doped with 1%, 3%, 5%, and 7% C were 7.77 nm, 7.64 nm, 12.37 nm, and 7.84 nm. Because of the uniform crystalline strains brought about by doping and the mismatch in ionic radii between the ions involved, shifting of the diffraction peaks was seen in this instance as the concentration of C increased. This coordination of the dopant ion with $ZnWO_4$ resulted in the formation of C;$ZnWO_4$. A number of diffraction peaks created at 5% and 7% were rather broad, whereas narrower peaks formed at 1% and 3%, indicating the material's monoclinic feature was eroding (Farha *et al*., 2022).

The diffraction peaks for the B doped $ZnWO_4$ nanocomposite were found at 2θ 18.90°, 24.57°, 36.32°, 36.43°, 41.32°, 52.53°, and 64.35 °. These match to the miller indices (100), (110), (020), (021), (121), (122), (221), (113), and (311). These crystal planes were identified as monoclinic phase of $ZnWO_4$. For the $ZnWO_4$ nanocomposite doped with B at 1%, 3%, 5%, and 7%, the average crystallite diameters were 12.60 nm, 7.25 nm, 14.44 nm, and 8.44 nm. The majority of the broad peaks in the 3% B doped $ZnWO_4$ material suggested that the material was tiny crystallite sized. As the boron concentration rose, the diffraction peak at 64.35° found in 1% B doped $ZnWO_4$, vanished. This is because B_7O may have formed. The nature of these dopants i.e. N, C, and B may be related to the reduction in crystallite size that occurs with doping. These dopants frequently diffuse and occupy the tungsten and zinc lattice layers, which have far larger ionic radii than the dopants, lowering the unit cell volume in every instance.

DOI: 10.56892/bima.v8i3B.844

Conversely, the ideal dopant concentration in each case was 7% Na, 7% Mg, 7% Ti, 7% N, 7% C, and 7% B doped $ZnWO_4$ nanocomposite, based on the crystallite size and, in particular, bandgap energy of the synthesised nanocomposites. Because of their smaller ionic radii, the other metal dopants are more easily able to penetrate the $ZnWO_4$ lattice than Na^+, which has a much greater radii and needs a higher concentration of dopant ions – at 7% for even the tiniest amount to come into contact with the lattice. Doping is primarily intended to improve the charge separation between electrons and holes in order to mitigate recombination rate-related issues. The surface area of the nanoparticles is increased by metal and nonmetal doping; this procedure is crucial for addressing the recombination problem since doping improves charge separation. Moreover, the increased surface area of the nanocomposites will boost their photocatalytic activity. Compared to undoped $ZnWO_4$, the doped nanocomposites exhibit higher levels of crystallinity because of the production of strong peaks (Geetha *et al*., 2019; Geetha *et al*., 2022). According to Bragg's law:

$$d(hkl)=\frac{nl}{(2sinu} \qquad \text{Equation 2}$$

In this case, the lattice parameters decrease as the diffraction angle u increases and its value is inversely related to the interplanar distance d. Diffraction peaks of ZnWO4 are consequently moved somewhat to a higher angle. The crystallite sizes were calculated using the Debye-Scherrer equation, which took into account the diffraction peak of greater intensity in each sample. Alkali ions C^{4-} entered the $ZnWO_4$ pores through structural destabilisation, forming the interstitial site. Meanwhile, N^{3-} ion formed coordinates with W^{6+} because of its larger ionic radius. B^{3+}, on the other hand, also coordinates with O^{2-} ions because of their difference in ionic radius and the fact that both elements share the same p orbital (Farha *et al.,* 2022).

CONCLUSION

This study investigated the effects of doping $ZnWO_4$ nanoparticles with non-metals N, C, and B on their bandgap energy, crystallinity, and photocatalytic activity. Using techniques like HRTEM, XRD, and SAED, both undoped and doped ZnWO4 nanocomposites were synthesized and analyzed for structural and optical changes. The results revealed significant reductions in bandgap energy, with the lowest values being 2.31 eV for N-$ZnWO_4$, 2.00 eV for C-$ZnWO_4$, and 2.30 eV for B-$ZnWO_4$. This decrease, attributed to new energy levels introduced by doping, is expected to improve solar energy conversion and photocatalytic efficiency. Each doped sample also exhibited distinct changes in crystallite size and lattice structure, with 7% doping found to optimize crystallinity and performance. The study recommends using 7% doping levels for N, C, and B to enhance the photoctlytic capabilities of $ZnWO_4$. Future work should explore co-doping methods and practical applications in photocatalysis, such as water purification and hydrogen production.

REFERENCES

Abubakar H. L., Tijani J. O., Abdulkareem S. A., Mann A., & Mustapha S. (2022). A review of the applications of zinc tungstate ($ZnWO_4$) photocatalyst for wastewater treatment. *Heliyon,* 8, e09964.

Abubakar H.L, Tijani J. O., Abdulkareem S. A., Egbosiuba T. C., Mann A., Mustapha S. & Ajiboye A. E. (2023). Effective removal of malachite green from local dyeing wastewater using zinc-tungstate based materials. *Heliyon,* 9, e19167.

Adesoye S., Abdullah S. A., Nwlin K. & Dellnger K. (2022). Mg-Doped ZnO Nanoparticles with tunable bandgaps for

DOI: 10.56892/bima.v8i3B.844

surface – enhanced raman scattering (SERS)-based sensing. *Nanomaterials*, 12, 3564.

Aga K. W., Efa M. T. & Beyene T. T. (2022). Effects of sulfur doping and temperature on the energy bandgap of ZnO Nanoparticles and their antibacterial activities, *ACS Omega*, 7, 12, 10796-10803.

Ali S. A. (2020). Application of Nanomaterials in Environmental Improvement. *IntechOpen*. doi: 10.5772/intechopen.91438

Chakraborty P.K., Mondal B.N. & Sardar G. (2021). Simple theoretical analyses of the Burstein–Moss shift (BMS) revisited for n-GaAs semiconductor with and without band-tailing conditions. *Indian Journal of Physics,* 95, 443–448. https://doi.org/10.1007/s12648-020-01730-6

Chen S. H., Wang B. X., Qiu X. H. & Xiong Z. S. (2013). Photoreactive Carbon and Nitrogen-Co doped $ZnWO_4$ Nanoparticles: Synthesis and Reactivity. *Advanced Materials Research, 621, 172–177.*

Dutta D. P. & Raval P. (2018). Effect of transition metal ion (Cr^{3+}, Mn^{2+} and Cu^{2+}) doping on the photocatalytic properties of $ZnWO_4$ nanoparticles. *Journal of Photochemistry and Photobiology A: Chemistry, 357, 193–200.*

Farha A. H., Al Naim A. F., Mazher J., Nasr O. & Alouane M. H. H. (2022). Structural and optical characteristics of highly UV-blue luminescent ZnNiO nanoparticles prepared by Sol-Gel method. Materials, 13(4), 879.Foo, K. Y., & Hameed, B. H. (2010). Insights into the modeling of adsorption isotherm systems. *Chemical Engineering Journal Journal*, 15(6), 2–10.

Geetha G. V., Keerthana S., Madhuri K. & Sivakumar R. (2021). Effect of solvent volume on the properties of $ZnWO_4$ nanoparticles and their photocatalytic activity for the degradation of cationic dye. *Inorganic Chemistry Communications*, 132, 108810.

Geetha G. V., R. Sivakumar R., Slimani Y., Sanjeeviraja C. & Kannapiran E. (2022). Rare earth (RE: La and Ce) elements doped $ZnWO_4$ nanoparticles for enhanced photocatalytic removal of methylene blue dye from aquatic environment, *Physica B : Condensed Matter,* 639, 414028.

Kumar P., Verma S., Korosin N. C., Zener B. & Stanger U. L. (2022). Increasing the photocatalytic efficiency of $ZnWO_4$ by synthesizing a $BiWO_6/ZnWO_4$ composite photocatalyst, *Catalysis Today*, 397-399, 278-285, ISSN 0920-5861.

Mourdikoudis S., Pallares R. M. & Thanh N. T. K. (2018). Characterization techniques for nanoparticles: comparison and complementarity upon studying nanoparticle properties, *Nanoscale,* 2018, **10**, 12871-12934

Rahmani M. & Sedaghat T. (2019) B. Nitrogen-doped $ZnWO_4$ nanophotocatalyst: synthesis, characterization and photodegradation of methylene blue under visible light. *Research on chemical intermediates,* 45, 5111-5124

Raizada P., Kumari J., Shandilya P. & Singh P. (2017). Kinetics of photocatalytic mineralization of oxytetracycline and ampicillin using activated carbon supported $ZnO/ZnWO_4$ nanocomposite in simulated wastewater. *Desalination and water treatment,* 79, 204 – 213.

Sagheer R., Khalil M., Abbas V., Kayani N. Z., Tariq U. & Ashraf F. (2020). Effect of Mg doping on structural, morphological, optical and thermal properties of ZnO nanoparticles, *Optik*, 200, 163428, ISSN 0030-4026.

DOI: 10.56892/bima.v8i3B.844

Sethi Y. A., Panmand R. P., Ambalkar A. A., Kulkarni A. K., Gunjal A., Gosavi S. W., Kulkarni V. M., Patil D. R. & Kale B. B. (2019). In situ preparation of CdS decorated $ZnWO_4$ nanorods as a photocatalyst for direct conversion of sunlight into fuel and RhB degradation. *Sustainable Energy & Fuels*, 3, 793-800.

Su Y., Chu H., Tin J., Du Z. & Xu W. (2021). Insight into the nanomaterials enhancement mechanism of nucleic acid amplification reactions, *TrAC Trends in Analytical Chemistry*, 137, 116221, ISSN 0165-9936.

Srinivasan S., Kannan A. M., Kothurkar N., Khalil Y., Kuravi S. (2016). Nanomaterials for energy and environmental application. *Journal of Nanomaterials*. 2015:2. Article ID: 979026

Tijani J. O., Abdullahi M. N., Bankole M. T., Mustapha S., Egbosiuba T. C., Ndamitso M., Abdulkareem A. S. & Muzenda E. (2021). Photocatalytic and toxicity evaluation of local dyeing wastetwater by aluminium/boron doped WO_3 nanopartiles. *Journal of Water Prcess Engineering*, 44, 102376.

Tijani J. O., Momoh U. O., Salau R. B., Bankole M. T., Abdulkareem A. S. and Roos W. D. (2019). Synthesis and characterization of $Ag_2O/B_2O_3/TiO_2$ ternary nanocomposites for photocaatlytic mineralization of local dyeing wastewater under artificial and natural sunlight irradiation. *Environmental Science and Pollution Research*, 26, 19942-19967.